Journal of Imaging Science and Technology® 50(1): 103–110, 2006.

Analysis of Friction-Induced Vibrations of a Xerographic Cleaning Blade

Yimei Yu
Technology & Development, Fuji Xerox Co., Ltd., 430 Sakai, Nakai-machi, Ashigarakami-gun, Kanagawa 259-0157, Japan

Abstract. *In this article, friction-induced vibrations of a xerographic cleaning blade are investigated theoretically and numerically. Using a finite element model, eigenvalue analysis of the blade vibration is conducted considering the friction force between the cleaning blade and the photoreceptor. It is indicated that two different mechanisms exist for the cleaning blade vibrations: the negative speed dependence of the friction coefficient and the friction induced coupling of certain vibration modes. Numerical analysis is carried out for a typical blade, and the unstable vibration modes are predicted for both mechanisms. Simulations are performed to verify the results of the eigenvalue analysis and to obtain additional results regarding the characteristics of the nonlinear vibrations in the time domain. The results are in agreement with vibrations observed in recent years in many xerographic cleaning subsystems. © 2006 Society for Imaging Science and Technology.*
[DOI: 10.2352/J.ImagingSci.Technol.(2006)50:1(103)]

INTRODUCTION

In many recent xerographic printers/copiers, a cleaning blade made from urethane rubber is used to remove untransferred toner and other particles from the photoreceptor surface before another cycle of printing/copying. The blade is typically fixed on a metal bracket through which the prescribed normal load is applied to compress the blade onto the surface of the rotating photoreceptor drum. A problem for the blade cleaning subsystem is the blade vibration caused by the friction between the blade and the photoreceptor.[1,2] The friction-induced blade vibration is essentially a self-excited vibration. It influences the cleaning subsystem performance, and can cause other problems such as noise and excessive wear of the blade and the photoreceptor.[3] Although the blade vibration can lead to severe failure of the cleaning subsystem, it is not fully investigated up to now. Research that focused on this subject is described in Ref. 2. In Ref. 2, the vibration of a cleaning blade was investigated using a single degree of freedom (1-DOF) model. It was indicated that the vibration was caused by the negative damping due to the negative speed dependence of the friction coefficient in the low slip-speed region.

Besides the vibrations described in Ref. 2, another class of vibrations were observed in recent years in several prototypes of high-speed printers under development. Although the blade configurations are somewhat different from each other for these prototypes, the vibrations have several characteristics in common which are apparently different from those described in Ref. 2, which suggests a possibility of a different mechanism for blade vibrations:

(1) The main resonance frequencies of the vibrations are in the range of 4–5 kHz, which are much higher than in Ref. 2 (where it is about 2.3 kHz).
(2) The vibrations occurred constantly at the normal process speed. In contrast, the vibrations in Ref. 2 arose just after the rotation of the photoreceptor drum started and just before it stopped, and it did not continue at a normal process speed.

Self-excited vibrations have been under investigation for a wide variety of mechanical systems for decades. It is well known that a multi-degrees-of-freedom (MDOF) system has a potential to be dynamically unstable (and as a result, self-excited vibration can occur) due to nonconservative force, which is formulated as asymmetric cross terms in the stiffness matrix. For example in rotor dynamics, rotor internal damping, including material damping and internal friction, and forces generated by fluid lubricants in journal bearings may be destabilizing depending on the rotational speed.[4,5] For many automotive braking systems such as a disk brake system[6–8] or a drum brake system,[9,10] friction force, which causes asymmetric coupling of dynamic modes, is a reason for self-excitation. Since the cleaning blade is essentially a MDOF system, it is possible that the same kind of self-excited vibration occurs. The purpose for this article is to give further investigation into the mechanism for the blade vibrations, especially the possibility of instabilities caused by dynamic coupling. The rest of the article is organized as follows. First, using a finite element model (which, being a MDOF model, gives better representation of the behavior of an actual blade compared to a 1-DOF one), the equation of motion for the blade is derived considering the friction force between the blade and the photoreceptor. Speed dependence of the friction coefficient is incorporated into the model. Next, through eigenvalue analysis, conditions for instability are discussed in the modal space of the nonfrictional system. It is indicated that both friction characteristics and dynamic coupling can drive the system to instability. Then, numerical analysis is conducted for a typical cleaning blade, and the unstable modes are predicted for both mechanisms. In the

Received Nov. 1, 2004; accepted for publication Feb. 8, 2005.
1062-3701/2006/50(1)/103/8/$20.00.

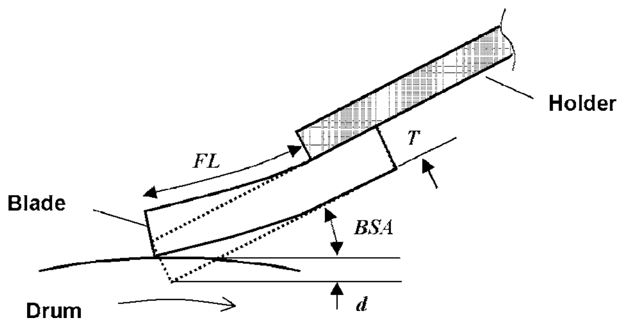

Figure 1. Configuration of a typical cleaning subsystem.

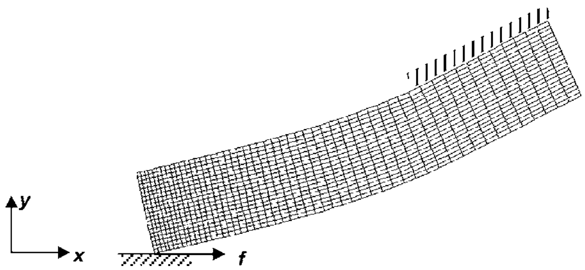

Figure 2. A finite element model.

final part of this article, simulations are performed to verify the results of the eigenvalue analysis and to further explore the characteristics of the nonlinear vibration in the time domain. It becomes clear that the self-excited vibration of the cleaning blade observed at a low-speed region is mainly caused by the friction characteristics, while that observed at a relatively high-speed region is mainly caused by dynamic coupling. The results are in agreement with vibrations observed in many cleaning subsystems in recent years.

MODELING OF THE VIBRATION SYSTEM

Figure 1 shows the configuration of a typical blade cleaning subsystem. The urethane blade is glued to a metal holder, which is, for example, fixed on the frame of the toner cartridge unit. The portion of the blade extending out of the holder is called the free length (FL), and the angle formed by the holder and the drum surface is called the blade setting angle (BSA). The blade has a thickness T. The dotted line in Fig. 1 shows the unstressed geometry of the blade, and with a positional interference d, the blade is compressed onto the drum surface with a normal load of a designed value. Since the system is uniform and long enough in the direction perpendicular to the plane shown, it will be treated as a plane strain problem.

In this article, a finite element model is used to approximate the behavior of the blade. Figure 2 shows an example of a finite element model with four-noded plane strain elements. The velocity at the drum surface (also called the process speed) is assumed to be constant. For the sake of simplicity, it is supposed that the only node that contacts the drum surface is the node at the edge of the blade. However, the following derivation can be easily generalized to a multinode-contact case. Both the holder and the drum are assumed to be rigid, thus a fixed boundary condition is applied to the portion of the blade surface glued to the holder, and with an assumption that the edge of the blade will not leave the drum surface, the movement at the edge is constrained in the direction y (see Fig. 2). The friction force that acts on the edge is first treated as an external force, and its influence on the system dynamics will become clear by the subsequent derivation. The force of gravity is neglected.

Linearized in the vicinity of the equilibrium state, that is, the steady sliding state, the blade dynamics can be described by the following n-dimensional second-order vector equation:

$$\boldsymbol{M}\ddot{\boldsymbol{X}}_r + \boldsymbol{C}\dot{\boldsymbol{X}}_r + \boldsymbol{K}\boldsymbol{X}_r = \boldsymbol{F}_r, \tag{1}$$

where $\boldsymbol{X}_r$ and $\boldsymbol{F}_r$ are, respectively, the displacement vector and the external force vector. The subscript r means that these vectors are variations from the equilibrium state instead of an unstressed state. $\boldsymbol{M}$, $\boldsymbol{C}$, and $\boldsymbol{K}$ are, respectively, mass, damping, and stiffness matrices. The modal matrix of the corresponding undamped, nonfrictional system is

$$\boldsymbol{\Phi} = (\phi_1, \phi_2, \ldots, \phi_n), \tag{2}$$

where $\phi_i (i=1,2,\ldots,n)$ is the ith mode shape vector, and $\boldsymbol{\Phi}$ is normalized with respect to the mass matrix. Assume proportional structural damping. Through a transformation

$$\boldsymbol{X}_r = \boldsymbol{\Phi}\boldsymbol{q}, \tag{3}$$

Eq. (1) can be rewritten in terms of the modal coordinate vector $\boldsymbol{q}$ as follows:

$$\boldsymbol{I}\ddot{\boldsymbol{q}} + 2\Sigma\Omega\dot{\boldsymbol{q}} + \Omega^2\boldsymbol{q} = \boldsymbol{\Phi}^T\boldsymbol{F}_r, \tag{4}$$

where $\boldsymbol{I}$ is the unit matrix of order n, and

$$\boldsymbol{q} = (q_1, q_2, \ldots, q_n)^T,$$

$$\Sigma = \mathrm{diag}(\zeta_1, \zeta_2, \ldots, \zeta_n),$$

$$\Omega = \mathrm{diag}(\omega_1, \omega_2, \ldots, \omega_n).$$

Assume that the displacement at the edge in the x direction (see Fig. 2) corresponds to the mth element of vector $\boldsymbol{X}_r$. From the one node contact assumption, we have

$$\boldsymbol{F}_r = (0, \ldots, 0, \overset{m}{\check{f}_r}, 0, \ldots, 0)^T,$$

where f_r is the variation (from the steady sliding state) of the friction force, and the cap over it indicates its index in the vector. Equation (4) then becomes

$$\boldsymbol{I}\ddot{\boldsymbol{q}} + 2\Sigma\Omega\dot{\boldsymbol{q}} + \Omega^2\boldsymbol{q} = f_r\boldsymbol{A}, \tag{5}$$

where

$$A = (\phi_{1m}, \phi_{2m}, \ldots, \phi_{nm})^T, \tag{6}$$

and $\phi_{im}(i=1,2,\ldots,n)$, whose value indicates how strongly the modal coordinate q_i is excited by the friction force, is the mth element of the ith mode shape vector ϕ_i.

Assume the friction coefficient is a function of the relative speed between the blade and the drum surface

$$\mu = \mu(|s|),$$

where $s = V_0 - \nu$, and V_0 and ν are the process speed and the speed at the blade edge, respectively. If the amplitude of the vibration is small enough that the direction of the relative speed keeps the same, then we have

$$f_r = \mu(V_0 - \nu)(N_0 + N_r) - \mu(V_0)N_0, \tag{7}$$

where N_0 is the reaction force (or, normal load) at the steady sliding state, and N_r is the variation. Recalling that the displacement at the edge corresponds to the mth element of vector $\boldsymbol{X}_r$, from Eqs. (3) and (6), we have

$$\nu = \boldsymbol{A}^T \dot{\boldsymbol{q}}. \tag{8}$$

Then $\mu(V_0 - \nu)$ can be expanded into the polynomial of $\dot{\boldsymbol{q}}$ as follows:

$$\mu(V_0 - \nu) = \mu(V_0) - \mu'(V_0)\boldsymbol{A}^T\dot{\boldsymbol{q}} + o(\dot{\boldsymbol{q}}). \tag{9}$$

Moreover, the reaction force variation N_r in Eq. (7) can be written in terms of modal coordinates as

$$N_r = \boldsymbol{B}^T \boldsymbol{q}, \tag{10}$$

where

$$\boldsymbol{B} = (b_1, b_2, \ldots, b_n)^T. \tag{11}$$

In Eq. (11), $b_i(i=1,2,\ldots,n)$ is the amplitude of the reaction force corresponding to a unit vibration of ith mode. More specifically, when the undamped, nonfrictional system is vibrating in its ith mode with $\boldsymbol{X}_r = \phi_i e^{i\omega_i t}$, the reaction force N_r will be $b_i e^{i\omega_i t}$. Equation (10) is true for a linear continuum and approximately true for a finite element model described by Eq. (1) when the elements at the contact area are small enough. Substituting Eqs. (9) and (10) into Eq. (7) and eliminating higher order terms, we have

$$f_r = -\mu'(V_0)N_0\boldsymbol{A}^T\dot{\boldsymbol{q}} + \mu(V_0)\boldsymbol{B}^T\boldsymbol{q}. \tag{12}$$

Consequently, from the earlier equation and Eq. (5), the dynamic equation of the frictional vibration system is derived as

$$\boldsymbol{I}\ddot{\boldsymbol{q}} + [2\Sigma\Omega + \mu'(V_0)N_0\boldsymbol{A}\boldsymbol{A}^T]\dot{\boldsymbol{q}} + [\Omega^2 - \mu(V_0)\boldsymbol{A}\boldsymbol{B}^T]\boldsymbol{q} = \boldsymbol{0}, \tag{13}$$

based on which the dynamic stability of the blade will be analyzed. From Eq. (13), the speed dependence of the friction coefficient causes an additional term to the damping matrix, and the friction itself causes an additional term to the stiffness matrix whether or not the friction is speed dependent. Since their nondiagonal elements are generally nonzero, the additional terms result in the coupling of the vibration modes. The damping matrix of the frictional system remains symmetric. However, if the friction-speed curve has a negative slope at V_0, i.e., $\mu'(V_0) < 0$, the damping matrix may become nonpositive-definite. In addition, the stiffness matrix of Eq. (13) is generally asymmetric. As a result, dynamic instability may occur.

FRICTION-INDUCED INSTABILITIES

The two factors, say, the negative speed dependence of the friction coefficient and the asymmetric coupling of vibration modes, together determine the stability of the frictional system. With the blade parameters and the friction characteristics given, stability of the frictional system can be analyzed by finding the eigenvalues of Eq. (13). The eigenvalues of Eq. (13) can be obtained, for example, by calculating the eigenvalues of the following matrix of the equivalent first order equations:

$$\begin{bmatrix} 0 & \boldsymbol{I} \\ -[\Omega^2 - \mu(V_0)\boldsymbol{A}\boldsymbol{B}^T] & -[2\Sigma\Omega + \mu'(V_0)N_0\boldsymbol{A}\boldsymbol{A}^T] \end{bmatrix}. \tag{14}$$

If there is any eigenvalue whose real part is positive, the system will be unstable. The imaginary part of the eigenvalue corresponds to the frequency of the unstable mode.

To get further insights into the problem, the following two special cases are investigated, specifically the cases when one of the aforementioned factors is dominant so that the influence of the other factor can be ignored.

Instability Due to Friction Characteristics

Consider the instability caused by the speed dependence of the friction coefficient. Neglecting coupling of the modes from Eq. (13), the equation of motion of modal coordinate $q_i(i=1,2,\ldots,n)$ can be approximated by

$$\ddot{q}_i + [2\zeta_i\omega_i + \mu'(V_0)N_0\phi_{im}^2]\dot{q}_i + [\omega_i^2 - \mu(V_0)\phi_{im}b_i]q_i = 0. \tag{15}$$

Since in general $\omega_i^2 \gg \mu(V_0)\phi_{im}b_i$, the above equation becomes unstable if its damping term is negative, or

$$\mu'(V_0) < -2\zeta_i\omega_i/(N_0\phi_{im}^2). \tag{16}$$

It is clear that the degree of instability of Eq. (15) increases with the negative derivative of the friction function and with the increasing of the normal load. This is consistent with the results in Ref. 2. Moreover, because the damping coefficient, ζ_i, is generally larger for high-order modes, low-order modes with larger $|\phi_{im}|$ have higher risk to become unstable. The physical meaning for this is that, it is easier for modes with larger displacement at the blade edge to be excited by the negative damping force caused by friction.

Instability Due to Dynamic Coupling

In order to investigate the influence of the friction-induced dynamic coupling on the stability of the system, assume the friction is *not* speed dependent. To assist in further understanding of the mechanism, consider the simplest case when

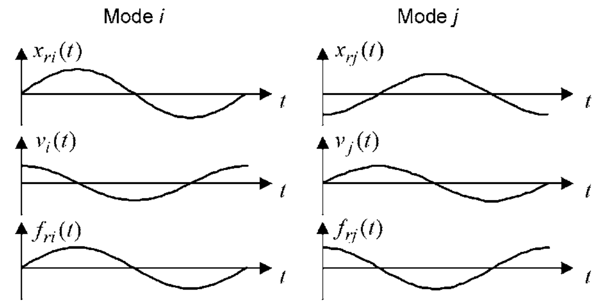

Figure 3. An example of two modes whose coupling causes instability.

two modes, say, the ith and the jth modes, of an undamped system are coupled by friction force. In this case, the equations of motion can be written as follows by an expansion of matrices in Eq. (13):

$$\begin{pmatrix} \ddot{q}_i \\ \ddot{q}_j \end{pmatrix} + \begin{bmatrix} \omega_i^2 - \mu\phi_{im}b_i & -\mu\phi_{im}b_j \\ -\mu\phi_{jm}b_i & \omega_j^2 - \mu\phi_{jm}b_j \end{bmatrix} \begin{pmatrix} q_i \\ q_j \end{pmatrix} = \begin{pmatrix} 0 \\ 0 \end{pmatrix}. \tag{17}$$

The eigenvalues for Eq. (17) can be derived analytically. After some manipulation, the condition for the system to be unstable can be obtained as

$$\mu^2(\phi_{im}b_i)(\phi_{jm}b_j) < -\frac{[(\omega_i^2 - \mu\phi_{im}b_i) - (\omega_j^2 - \mu\phi_{jm}b_j)]^2}{4}, \tag{18}$$

or approximately

$$\mu^2(\phi_{im}b_i)(\phi_{jm}b_j) < -\frac{(\omega_i^2 - \omega_j^2)^2}{4}. \tag{19}$$

It can be easily verified that when Eq. (17) becomes unstable, the imaginary parts of the eigenvalues, and accordingly the frequencies of the modes of the frictional system will become equal, while the real parts of the eigenvalues will be equal in absolute value but with opposite sign.

In contrast to inequality (16), which is a condition on the derivative of the friction-speed function, inequality (19) is a condition on the amount of the friction. From inequality (19), for instability to occur, it is required that the two modes have the following properties:

(1) $\phi_{im}b_i$ and $\phi_{jm}b_j$ are of opposite sign and
(2) the frequencies of the modes are close enough.

To help understand the meaning of these two conditions, a conceptual diagram is shown in Fig. 3 of an example of two modes that satisfy the earlier requirements. Without loss of generality, assume $\phi_{im}b_i$ is positive and $\phi_{jm}b_j$ is negative. In addition, for the sake of simplicity, assume the frequencies of these two modes are almost equal. If mode i is excited slightly by some noise, a displacement variation $x_{ri}(t)$ and a friction variation $f_{ri}(t)$ will be generated at the edge of the blade. Since $\phi_{im}b_i$ is positive, $f_{ri}(t)$ will be of the same phase as $x_{ri}(t)$ [refer to the definition of b_i below Eq. (11)]. The force variation $f_{ri}(t)$ then excites mode j and causes a displacement variation $x_{rj}(t)$ with a phase lag of about $\pi/2$. The vibration of mode j will produce a friction variation $f_{rj}(t)$, which, with a phase reversing that of $x_{rj}(t)$ (recalling $\phi_{jm}b_j$ is negative), in turn excites mode i. In Fig. 3, $\nu_i(t)$ and $\nu_j(t)$ are velocities corresponding to $x_{ri}(t)$ and $x_{rj}(t)$. From Fig. 3, $f_{rj}(t)$ and $\nu_i(t)$ are of the same phase, and it is the same with $f_{ri}(t)$ and $\nu_j(t)$. Thus, because of the existence of friction, these two modes do positive work on each other, and as a result the vibration grows, which consequently causes instability. This is the physical explanation of instability caused by dynamic coupling of vibration modes.

Table I. Natural vibrations in the absence of friction.

Mode i	Frequency (Hz)	Eigenvalue real part	ϕ_{im} (m)	b_i (N/m)
1	1164	-5.35×10^1	-0.16	-3.22×10^6
2	2186	-1.89×10^2	10.18	-3.79×10^6
3	3162	-3.95×10^2	0.99	-1.78×10^7
4	4944	-9.65×10^2	4.30	-2.77×10^7
5	5339	-1.13×10^3	-5.37	-1.14×10^7
6	6651	-1.75×10^3	-7.27	-1.78×10^7
7	7333	-2.12×10^3	1.43	-1.87×10^7
8	9059	-3.24×10^3	11.61	1.28×10^7

NUMERICAL ANALYSIS FOR A TYPICAL BLADE

Consider a typical cleaning blade with the following parameters: FL=8 mm, T=2 mm, BSA=25 deg, d=1.2 mm, E $=8.0\times10^6$ N/m^2, DEN$=1.5\times10^3$ kg/m^3, where E is the Young's modulus, and DEN is the mass density of the urethane rubber. Moreover, suppose the blade is stiffness proportional damping. That is, for the damping matrix $\boldsymbol{C}$ in Eq. (1), we have

$$\boldsymbol{C} = \beta\boldsymbol{K}. \tag{20}$$

A value 2.0×10^{-6} s, which is approximately estimated from the rubber's rebound resilience, is assumed for damping factor β in the following numerical analyses and simulations.

With the friction coefficient $\mu(V_0)$ given, the blade deformation at steady sliding is first calculated. Then the natural vibrations in the absence of friction are calculated in the vicinity of the steady sliding state. The results for the first eight modes are given in Table I (the friction coefficient is assumed to be 0.7 when calculating the deformed shape at steady sliding). The unit of b_i is N/m because this is a plane strain problem. The eigenvalue real parts are simply $-0.5\ \beta\omega_i^2$ from the stiffness proportional damping assumption. Modes of higher order are not considered since, in general, the high-order modes are only minimally excited. The mode shapes for the first five modes are shown in Fig. 4,

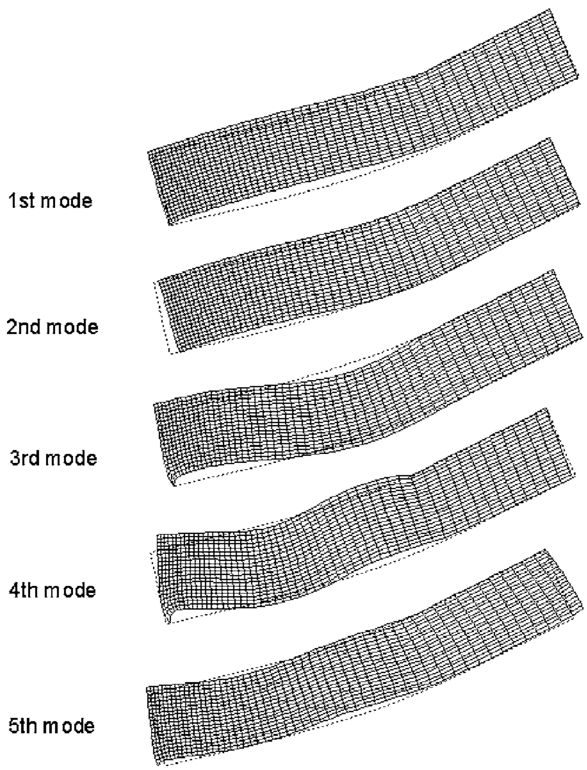

Figure 4. *Modal shapes of the blade in the absence of friction.*

in which the dotted lines correspond to the shape of the blade at steady sliding. It is clear that the first and the third modes are dominated by bending vibrations. For these two modes, the displacements at the edge of the blade are very small. On the other hand, the second mode is more affected by longitudinal vibration, thus, the displacement at the edge for the second mode is larger compared with other modes. This can be seen from the values of ϕ_{im} in Table I, too. From inequality (16), it can be easily verified that the second mode is more likely to become unstable than other modes if the friction coefficient is negative speed dependent. Referring to Table I, the frequency of the second mode is about 2.2 kHz. This value corresponds approximately with the frequency in Ref. 2 of the vibration due to the speed dependence of friction.

Since there was much investigation in Ref. 2 concerning the instability due to the speed dependence of friction, further discussion is omitted here. Instead, a detailed investigation is performed concerning the instability due to dynamic coupling of vibration modes.

Assume a constant friction coefficient $\mu=0.7$. From the instability conditions and a simple observation of the modal information given in Table I, the forth and the fifth modes are most likely to be coupled to cause instability when coupling of the neighboring two modes is considered (however, this does not exclude the possibility of other unstable coupling). For eigenvalue calculation, a higher-order model is used considering all of the first eight modes. The results are given in Table II. From Table II, the fourth mode has an eigenvalue with positive real part. This indicates that for $\mu=0.7$, the frictional system is dynamically unstable at a frequency of about 5.2 kHz. This frequency corresponds approximately with that observed in the prototypes. A comparison of Tables I and II shows that, eigenvalues of the fourth and the fifth modes move in the opposite direction. While the fourth mode becomes unstable, the fifth mode becomes more stable. Also, the frequencies of these two modes become nearly equal. For other modes, the eigenvalue real parts remain almost unchanged, although for some of them, specifically the modes with large displacement at the edge, the frequencies are affected by the existence of friction. Thus, as predicted, friction-induced coupling of the fourth and the fifth modes can lead to the instability of the system. On the other hand, stabilities of the other modes are only slightly affected.

Table II. Eigenvalues of the frictional system with $\mu=0.7$.

Mode	Frequency (Hz)	Eigenvalue real part	Eigenvalue imaginary part
1	1161	-5.34×10^{1}	7.29×10^{3}
2	2331	-1.90×10^{2}	1.46×10^{4}
3	3218	-3.93×10^{2}	2.02×10^{4}
4	5205	$+1.27\times10^{2}$	3.27×10^{4}
5	5212	-2.21×10^{3}	3.27×10^{4}
6	6455	-1.76×10^{3}	4.05×10^{4}
7	7358	-2.12×10^{3}	4.62×10^{4}
8	8905	-3.24×10^{3}	5.59×10^{4}

To investigate the influence of the friction coefficient on the system instability, eigenvalue analyses are performed using different values of friction coefficients, and the results are shown in Fig. 5. It can be seen that when μ is small, the eigenvalue real parts of these two modes remain almost unchanged, and the dynamic coupling works to get the frequencies closer. When μ reaches about 0.35, the real parts start to separate, and of these two modes, the real part of the fourth mode moves toward the unstable region. At the same time, the frequencies become even closer and nearly equal. At a value $\mu\approx0.64$, the eigenvalue real part of the fourth mode crosses the horizontal axis. Thus, for the current blade, the frictional system is unstable for $\mu>0.64$, and the degree of instability increases with increasing of μ.

SIMULATION RESULTS

Because the problem is essentially nonlinear, the unstable vibration will not grow infinitely, but will develop into a limit cycle oscillation instead. Although eigenvalue analysis can predict the unstable modes, many characteristics in time domain of the resultant vibration cannot be obtained by simply performing eigenvalue analysis. In this section, simulations are conducted to verify the analyses results and to give further investigation into the characteristics of the non-

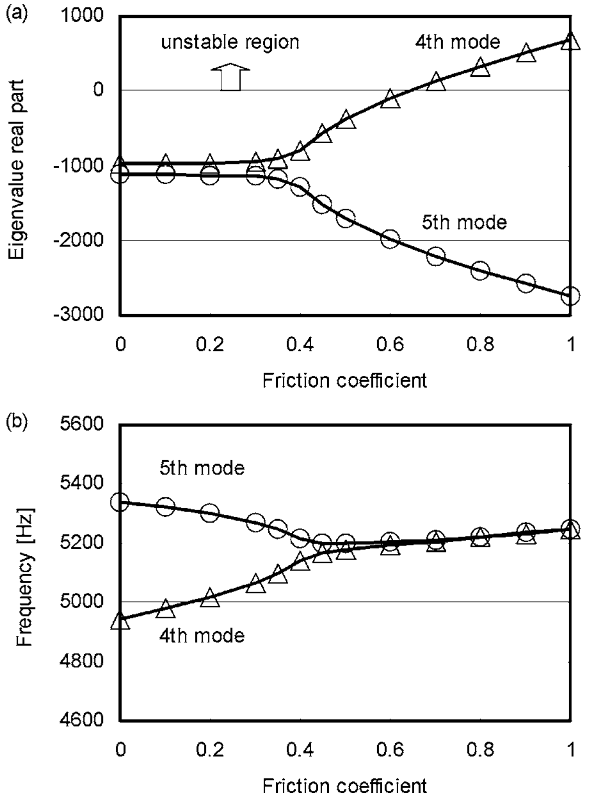

Figure 5. (a) Eigenvalue real parts and (b) frequencies as functions of friction coefficient.

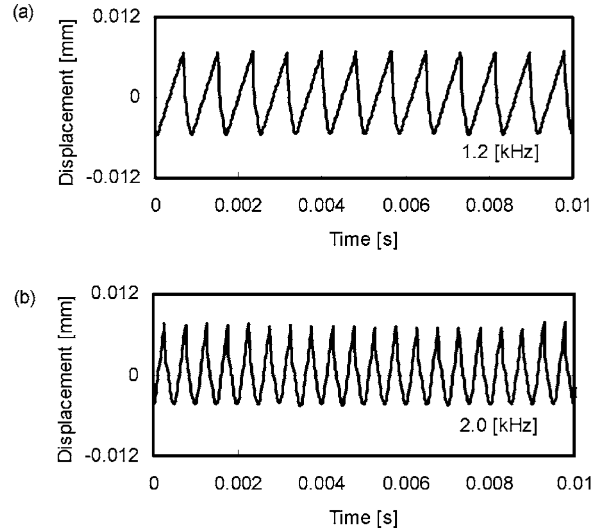

Figure 6. Time histories of the displacement at the blade edge of vibrations due to speed dependent friction, for process speeds (a) 20 and (b) 50 mm/s.

linear vibration. The *ABAQUS* nonlinear finite element program was used during the simulations. The blade and the photoreceptor drum are first modeled at positions without interference. Then the behavior of the blade is simulated by a direct integration over time. The simulation procedure is as follows:

Step 1. Compress the blade to the photoreceptor drum surface by a prescribed displacement, with the movement of the drum constrained.
Step 2. Start up the rotation of the drum, until the prescribed process speed is achieved.
Step 3. Keep the drum rotating with a constant speed.

The movement of the blade edge when the drum is rotating constantly is sampled and analyzed later.

Case 1

Consider the vibration caused by the negative speed dependence of friction. Assume a friction coefficient that decays exponentially with slip speed

$$\mu(|s|) = \mu_\infty + (\mu_0 - \mu_\infty)\exp(-\gamma|s|), \tag{21}$$

where $\mu_0=0.4$, $\mu_\infty=0.3$, and $\gamma=0.8$. Figure 6 shows the time histories of the displacement at the edge when the process speed is 20 and 50 mm/s, respectively. The corresponding oscillation frequencies are given alongside. The origin of the time axis is shifted to a specific time step during step 3 when the amplitude of the oscillation converges to a certain value. It can be seen that in both cases the motions are stick-slip vibrations, which usually occur for systems with variation of frictional resistance. For a very low process speed, say, 20 mm/s, the frequency of the vibration deviates from that of the second mode, because in this case the frequency is determined mainly by the duration of the stick period. However, the frequency approaches that of the second mode when the process speed is 50 mm/s. It is confirmed that vibrations do not occur for process speed 60 mm/s and higher.

Case 2

Consider the vibration caused by the dynamic coupling of vibration modes. Assume a constant friction coefficient $\mu=0.7$. It is predicted in the previous section by eigenvalue analysis that the system is unstable at a frequency of about 5 kHz. This vibration is observed in the simulation result. Figure 7 gives the time histories of the displacement and velocity at the blade edge for a process speed 200 mm/s. It is noted that, although the friction coefficient is assumed to have a constant value, the motion is a typical stick-slip oscillation.

Figure 8 shows the time histories of the displacement at the edge of the blade for different values of process speed between 50 and 200 mm/s. For the sake of clarity, the curves have been shifted vertically by the amounts 0.11, 0.07, 0.04, and 0.01 (from the upper to the lower curve), respectively. It is clear that the amplitude of the vibration increases with the process speed, while the frequency of the vibration keeps almost the same for the current range of process speed.

From the earlier simulation results, the vibrations of the blade caused by the two different mechanisms occur at different process speed ranges. The vibrations due to the characteristics of friction occur mainly in the low speed regime.

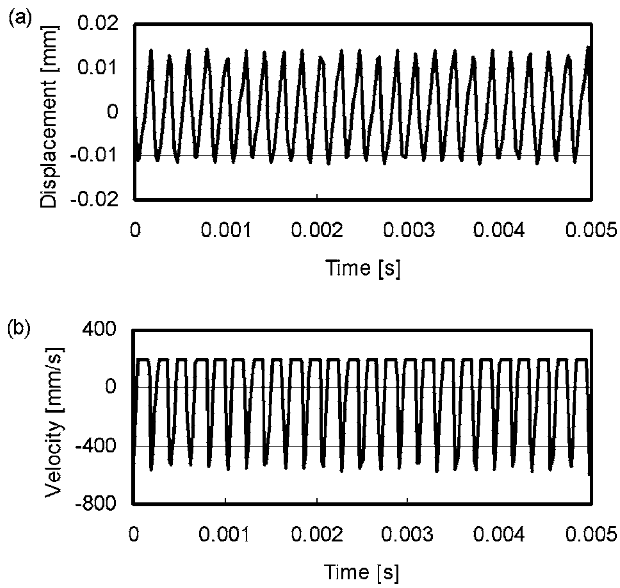

Figure 7. Time histories of (a) the displacement and (b) the velocity at the blade edge, of the vibration due to dynamic coupling of vibration modes.

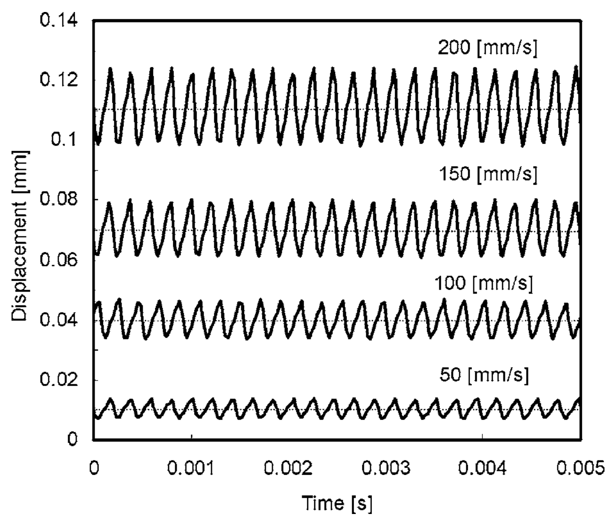

Figure 8. Time histories of the displacement at the blade edge for different values of process speed, of vibrations due to dynamic coupling of vibration modes.

For a typical blade, the second mode is excited and the frequency of the vibration is relatively low. On the other hand, the vibrations due to dynamic coupling grow with the process speed. For a typical blade, the coupling of the fourth and the fifth modes can cause instability, and the frequency of the vibration is relatively high. Because the process speeds of printers/copiers are becoming higher and higher, vibrations caused by the dynamic coupling occur more frequently than before. This explains why in many cases the vibrations observed in the prototypes being developed nowadays have frequencies higher than those observed a decade ago.

Case 3

So far the vibrations caused by the two mechanisms are investigated independently. It is natural to ask what will happen if both mechanisms work. To investigate this, assume a velocity dependent friction coefficient as expressed by Eq. (21) but with $\mu_0=0.8$ and $\mu_\infty=0.7$. Thus, in this case, the friction coefficient has the same speed dependence as in case 1, and it has the same value at the high-speed region as in case 2. Therefore, there is possibility that both mechanisms work. Simulations are performed for process speeds 20, 50, and 200 mm/s, respectively, and the results are given in Fig. 9. For the sake of clarity, the curves have been shifted vertically by the amounts 0.09, 0.05, and 0.02 (from the upper to the lower curve), respectively. Comparing the results with those of cases 1 and 2, we can see that, for a low process speed of 20 mm/s, the vibration is dominated by the speed dependence of friction (the frequency is somewhat higher than in case 1 because the amplitude in this case is smaller due to larger friction resistance and accordingly the period of stick phase is shorter), while for a high process speed of 200 mm/s, the vibration is dominated by the coupling of vibration modes. This is consistent with the results from cases 1 and 2 concerning the relation between the vibration mechanisms and the process speed. For the process speed 50 mm/s, the vibration is more complicated due to the influence from both factors. Because the stick-slip motion is highly nonlinear, the motion is far from a superposition of two vibrations with different frequencies. The stick and the slip periods occur by a frequency of 3 kHz, which is in between the frequencies of the vibrations for process speeds 20 and 200 mm/s, while the amplitude of the oscillation varies over time. Note that the frequency is close to that of the third mode. Thus, the possibility of a resonance of the third mode cannot be excluded, although it is clear from the eigenvalue analysis that the third mode by itself can hardly go unstable. Further investigation is needed in the future research concerning the nonlinear behavior of the blade when both mechanisms work.

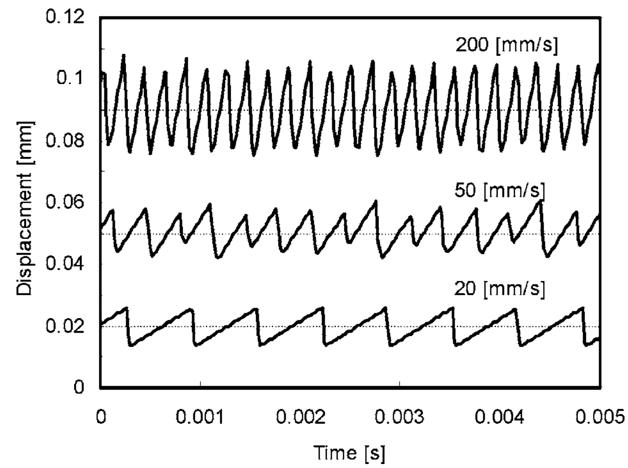

Figure 9. Time histories of the displacement at the blade edge for different values of process speed when both mechanisms may work.

CONCLUSIONS

In this article, friction-induced vibrations of a cleaning blade are investigated theoretically and numerically. Using a finite element model, the eigenvalue analysis of the blade vibration is conducted considering the friction force between the cleaning blade and the photoreceptor. It is indicated that, depending on the blade dynamics and the friction characteristics, the blade vibrations can be caused by two different mechanisms: the negative speed dependence of the friction coefficient, and the friction-induced coupling of vibration modes. Numerical analysis and simulations are preformed for a typical cleaning blade. It is shown that, for the first mechanism, primarily the second mode of the blade is excited. The vibration occurs mainly in the low-process-speed range. While for the second mechanism, the instability is most likely to be caused by the coupling of the forth and the fifth modes. The vibration tends to occur at rather higher process speeds. These results are in agreement with vibrations observed in recent years in many xerographic cleaning subsystems.

ACKNOWLEDGMENT

The author wishes to thank Hidetoshi Takahashi for supporting the initial development of the *ABAQUS* finite element model.

REFERENCES

[1] N. Lindblad, *Proc., IS&T's 10th International Congress on Advances in Non-Impact Printing Technology* (IS&T, Springfield, VA, 1994) p. 64.
[2] H. Kawamoto, J. Imaging Sci. Technol. **40**, 8 (1996).
[3] K. Seino and S. Yuge, J. Imaging Sci. Technol. **47**, 424 (2003).
[4] A. Tondl, *Some Problems of Rotor Dynamics* (Chapman and Hall, London, 1965).
[5] J. Melanson and J. W. Zu, J. Vibr. Acoust. **120**, 776 (1998).
[6] J. D. Fieldhouse and P. Newcomb, *SAE Paper 930805* (1993).
[7] A. Sueoka, T. Ryu, and K. Shirozu, Trans. Jpn. Soc. Mech. Eng., Ser. C **67**, 1727 (2001) (in Japanese).
[8] S. Kung, K. B. Dunlap, and R. S. Ballinger, *SAE Paper 2000–01–0444* (2000).
[9] J. Hulten, *SAE Paper 932965* (1993).
[10] K. Satou, F. Hara, and M. Watanabe, Trans. Jpn. Soc. Mech. Eng., Ser. C **64**, 1485 (1998) (in Japanese).